Impact of γ-radiation on carbon steel anaerobic corrosion and H2 production.

Stavroula Isidora Giannakandropoulou, Hortense Desjonqueres, Charles Wittebroodt, Gérard Baldacchino

"Impact of γ-radiation on carbon steel anaerobic corrosion and H_2 production."

Authors list / affiliations

Stavroula-Isidora Giannakandropoulou[1,3], Hortense Desjonqueres[1], Charles Wittebroodt[2*], Gérard Baldacchino[3]

[1]Institut de Radioprotection et de Sûreté Nucléaire (IRSN), PSN-RES/SCA/LECEV, 91191, Gif-sur-Yvette, France; [2]Institut de Radioprotection et de Sûreté Nucléaire (IRSN), PSE-ENV/SEDRE/LETIS, 92260, Fontenay-aux-Roses, France; [3]Université Paris-Saclay, CEA, CNRS, LIDYL, 91191, Gif-sur-Yvette, France.

Abstract

This article reports investigations on the anoxic corrosion process impacting a carbon steel/ultrapure deaerated water system when it is exposed to gamma radiation (50 Gy h^{-1}), and on the associated molecular hydrogen gas generation. On the one hand, a dynamic semi-open experimental setup allowing to distinguish between the H_2 production related to water radiolysis and the one related to anoxic corrosion has been adopted to estimate the corrosion rate associated to three successive temporal phases: pre-irradiation, irradiation and post-irradiation phases. On the other hand, *post mortem* analyses performed on both liquid and solid samples permitted to (i) quantify the chemical changes occurring in solution due to the formation of water radiolysis products and (ii) observe and characterize the thin corrosion layer composed of magnetite (Fe_3O_4) at the surface of the metallic coupons. We show that gamma radiation induces a slight diminution of the carbon steel corrosion rate. However, by comparing the mean corrosion rate values obtained for the three studied phases (i.e., before, during and after irradiation), the chemical changes caused by radiolytic species seem to inhibit the formation of a thick magnetite protective layer. Additionally, the corrosion rate observed in post-irradiation phase does not decrease over time, which suggests that irradiation could modify the properties of the corrosion product

* Corresponding author. *Email address*: charles.wittebroodt@irsn.fr (C. Wittebroodt).

layer by making it less protective. A structural modification of this oxide film might be caused by the oxidizing water radiolysis products. Such mechanisms may favour continuous active corrosion processes rather than passivation of the metallic surface and thus lead to a reduced lifetime of the component.

Keywords

Anoxic corrosion; carbon steel; water radiolysis; γ-rays; hydrogen production

1. Introduction

Deep geological disposal of high-level radioactive waste (HLW) is foreseen by several countries to protect living organisms from long-term radioactive contamination [1,2]. In France, according to the multi-barrier concept developed by Andra (French radioactive waste management agency), HLW would be embedded in a glass matrix cooled in a stainless steel container. This package would be then encapsulated into cylindrical carbon steel overpack and inserted in a carbon steel casing tube within horizontal micro-tunnel drilled in the highly impermeable Callovo-Oxfordian (COx) clay rock of the Paris Basin [3,4]. A bentonitic cement-based grout material would be injected between the steel casing and the host rock in order to (i) neutralize the acidity coming from pyrite oxidation in the COx while preserving glass from detrimental highly alkaline media, (ii) limit oxygen diffusion and microbial activity and (iii) passivate the steel casing. If carbon steel casing should ensure adequate mechanical function over a century to allow the nuclear waste to be retrieved from the deep geological disposal concept, carbon steel overpack must remain leakproof for a few thousand years to prevent natural clayey porewater seeping from the host rock from reaching the vitrified waste during the thermal phase [4]. Throughout the duration of the operational phase of the project and long after the closure of the disposal facility, several corrosion processes are expected to occur in a series of distinct environments (i.e., in oxic or anoxic conditions, in contact with liquid or vapour phase solution, in contact with solution whose chemical composition evolves over time due to the continuous percolation of clayey porewater through the bentonitic cement grout material) which will gradually impair the carbon steel and finally induce mechanical failure of the metallic component [5]. Predominant over the long term, carbon steel anoxic

corrosion process will progressively attack the metallic elements, with a mean corrosion rate value between 0.1-10 µm year^{-1} [3,6–8]. Under these conditions, iron will interact with water to produce ferrous hydroxide ($Fe(OH)_2$) and hydrogen gas (H_2):

$$Fe + 2\,H_2O \rightarrow Fe(OH)_2 + H_2 \quad (1)$$

When the Schikorr reaction (reaction 2) occurs, ferrous hydroxide ($Fe(OH)_2$) can be then transformed to the more thermodynamically stable magnetite (Fe_3O_4):

$$3\,Fe(OH)_2 \rightarrow Fe_3O_4 + 2\,H_2O + H_2 \quad (2)$$

In natural or artificial porewater, or in presence of bentonite, iron can react with dissolved species to form other corrosion products such as siderite ($FeCO_3$) through the overall reaction:

$$Fe + 2\,MHCO_3 \rightarrow FeCO_3 + H_2 + M_2CO_3 \quad (3)$$

where M is a balancing univalent cation [9]. As shown in reactions (2) and (3), anoxic corrosion process will produce magnetite and/or siderite as main corrosion products and generate significant amounts of hydrogen. Thus, such anoxic corrosion processes induce corrosion products the formation of corrosion products leading to the progressive protection of the metallic surface. However, this beneficial phenomenon is always accompanied by the production of H_2 gas whose accumulation may significantly affect mid- and long-term safety of the disposal facility. On the one hand, its high flammable and explosive properties represent a risk during the operational phase and on the other hand, the consequent overpressure is liable to lead to incomplete saturation of bentonite sealing plugs aiming at mitigating the migration of radionuclides through disposal installation [5-9]. In addition, it is noteworthy that all these corrosion processes will take place on carbon steel component exposed to ionizing radiations originating from nuclear waste. These radiations will lead to the radiolysis of percolated porewater which forms radiolytic species such as radicals (e^-_{aq}, $H^\bullet$,$^\bullet OH$), molecular products (H_2O_2, H_2) and ionic species (H_3O^+), according to reaction (4) [10-11]:

$$H_2O \rightarrow e^-_{aq}, H^\bullet, {}^\bullet OH, H_2O_2, H_2, HO_2^\bullet, H_3O^+ \quad (4)$$

These chemical species, whose concentrations are dependent on LET (Linear Energy Transfer, defined as the amount of energy deposited by the charged particle along its path in solution) are prone to modify the physico-chemical conditions at the metal-water interface, and thus to impact the corrosion processes and the associated corrosion rate. Furthermore, these formed radiolytic species include H_2 gas, meaning that porewater radiolysis will also lead to the additional production of this problematic gas [5,12-13].

Therefore, to contribute to the long-term safety assessment of such deep geological disposal, dedicated research programs have been committed to study steel corrosion under irradiation and the associated hydrogen gas production. The various experimental techniques that have been used to measure uniform corrosion rates can be grouped as follow: weight loss measurements [13], hydrogen gas production monitoring [14] and electrochemical measurements [15]. While a range of individual studies has been performed to understand the impact of several parameters such as the dose rate (or total dose), the temperature or the physico-chemical properties of the solution, the observed effects of ionizing radiation on steel corrosion are still conflicting. Even though, most studies demonstrate that carbon steel corrosion rate is enhanced by radiation exposure [13,16-17], some others tend to indicate the contrary [18–20]. In parallel, while a large majority of the works cited above agreed on the fact that magnetite (Fe_3O_4) is the predominant corrosion product which is formed under such experimental conditions, many key questions regarding the mid and long term evolution of this oxide film properties, induced by the physico-chemical modifications of the solution caused by irradiation, remain unanswered.

The primary motivation of the work presented in this article is to investigate the impact of gamma radiation on carbon steel anoxic corrosion processes in order to (i) quantify the H_2 production and (ii) estimate the associated corrosion rate allowing an optimisation of the metallic elements design. As an initial approach, ultrapure deaerated water has been used in order to study a simplified system allowing to capture the main radiolytic processes that could influence the corrosion processes. While almost all studies dealing with the impact of ionizing radiations on steel corrosion processes have been performed in closed systems, the present work is meant to get closer to the real disposal conditions by working in a semi-open system. This experimental setup allows to distinguish between the H_2 production related to water radiolysis and the one related to anoxic corrosion, making possible the estimation of associated

corrosion rate. Finally, *post mortem* analysis are performed on the metallic samples surface to identify neoformed corrosion products, and chemical characteristics of the solution are determined.

2. Materials and Methods

2.1. Experimental setup

A schematic overview of the innovative dynamic experimental set up used in this work to study the impact of gamma radiation on anoxic corrosion of steel processes is given in Figure 1. It allows to differentiate the hydrogen production attributed to anoxic corrosion and the one imputed to radiolytic process, by measuring continuously the H_2 gas generated by two parallel systems: one cell containing six carbon steel samples immersed in pure deaerated water, the other cell containing only pure deaerated water. These two stainless steel cells are placed into an irradiation chamber where they are exposed to gamma-radiation and their H_2 evolution is recorded using in-line gas chromatography. This paper reports the results associated with two successive series of experimental tests (Exp-A and Exp-B) where hydrogen production is monitored before, during and after irradiation under anoxic conditions and at ambient temperature.

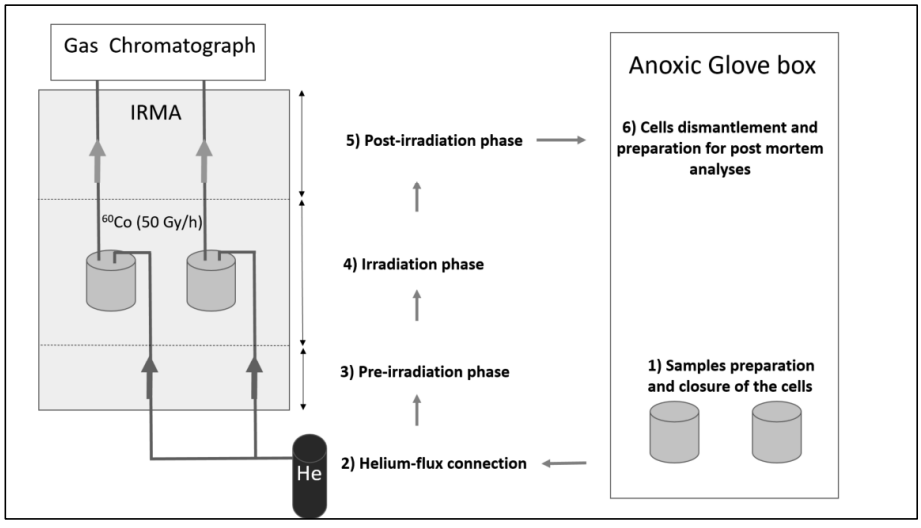

Fig. 1: Schematic view of the experimental set-up and presentation of the adopted procedure, from the preparation and closure of the cells until their dismantlement.

2.2. Experimental procedure

Corrosion experiments are performed on coupons (50 x 10 x 1 mm) of commercially available S235 carbon steel (max. 0.17 wt% of C, 1.40 wt% of Mn, 0.03 wt% of Sb, 0.02 wt% of P, 0.02 wt% of S). To minimize the amount of surface oxide present before the start of Exp-A, four metallic samples are roughly polished using #220 and #1200 SiC paper ("AR-coupons"), and two other samples are further polished using diamond paste, obtaining a smooth mirror surface ("AP-coupons"). For Exp-B, the six metallic samples are roughly polished ("BR-coupons") with the same procedure described above. After polishing, which takes place only few hours before the experiment, the samples are cleaned for 10 minutes with ethanol in an ultrasonic bath and then they are let to dry. For experimental system involving metallic samples (A1-cell and B1-cell), the six coupons are inserted in a dedicated borosilicate glass sample holder which allow to maximize the carbon steel surface available for corrosion processes. The sample holder is then introduced in a borosilicate glass beaker containing a volume of 200 mL of ultrapure (Millipore Alpha-Q with an electrical resistivity of 18.2 MΩ) deaerated water sufficient to ensure a total immersion of the coupons. The beaker is then emplaced in a stainless steel cell made up of a cylindrical body (10.4 cm, r =11cm) and a cover fitted with a tin seal allowing it to be hermetically closed. The cell cover is fitted with two stainless steel line allowing the circulation of a carrier gas. The input line has a sufficient length to get into the solution contained in the beaker whereas the output line internal extremity is located at the same level as the beaker upper part (Figure 2). Both lines are equipped with a valve on their external part to avoid any unintended oxygen contamination during cells transportation. In parallel, experimental system dedicated to ultrapure deaerated water radiolysis study (A2-cell and B2-cell) is prepared following the same procedural steps as in the case of experimental system involving metallic samples, except the introduction of the sample holder containing the coupons. To ensure that inert atmosphere prevail in our experimental cells and to avoid any further oxidation of the metallic coupons, all these preparation processes are performed in an anoxic glove box under

147 continual nitrogen (N_2) flow. Once the cells are closed their tightness is checked via leak detector
148 (Leybold Infinicon, UL 200).

149

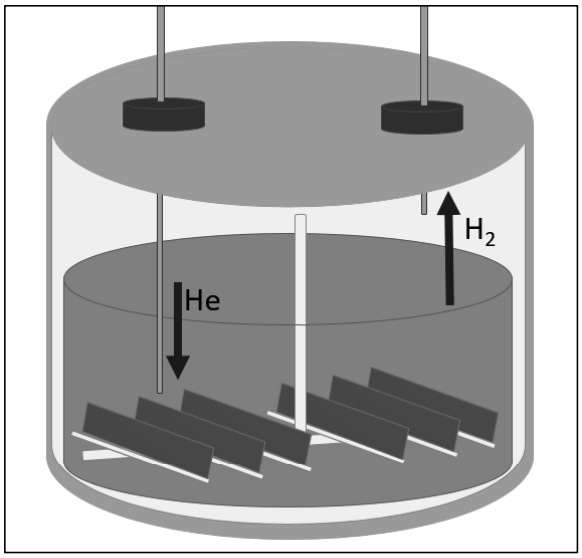

150

151 **Fig. 2**: Schematic view of a stainless steel cell containing carbon steel samples (cell A1 & B1). Metallic
152 coupons, sample holder and pure deaerated water are placed into a glass beaker before entering the cell.

153

154 2.3. Irradiation experiments

155 Each experimental test involves two cells: a first one containing ultrapure deaerated water and metallic
156 samples and a second one containing only ultrapure deaerated water. After their preparation under inert
157 atmosphere, both cells are hermetically closed and carried from the glove box to the irradiation chamber
158 of IRMA (IRradiation MAterials) facility, of the Institute for Radiological Protection and Nuclear Safety
159 (IRSN), located at Saclay research center. The IRMA facility, by design, allows on-line measurements
160 during the irradiation phases. Thanks to the input/output lines, the cells are then connected to the
161 circulation system making possible to inject a carrier gas into the solution (input line) and to flow
162 continuously the produced hydrogen gas towards a gas chromatograph (output line) *via* flow-controllers,
163 set at 5 ml min^{-1}. In IRMA facility, materials are submitted to gamma radiation thanks to four cylindrical

sealed sources of ^{60}Co (T½ = 5.27 years). At the date of the experiments, the total activity of the sources was about 774 TBq and 684TBq for Exp-A and Exp-B, respectively. In order to achieve an estimation of the real conditions that would prevail in a repository environment, a rather low dose rate of 50 Gy h^{-1} (corresponding to approximately five times to the predicted *in situ* dose rate) is applied. The calculations of the theoretical distances between the sources and the cells, required to obtain the desired dose rate, were carried out with a dedicated software (Microshield® 9.07). These distances are afterwards validated by measuring the dose rate using a calibrated ionization chamber, at the defined locations, in the presence of radioactive sources. Hence, the cells were placed about 1 m from the sources support, behind a 5 cm width steel shield for Exp-A and a 2 cm width lead shield for Exp-B. For Exp-A and Exp-B, the duration of the test under irradiation was 15 and 16 days respectively, corresponding to a total absorbed dose of 18 and 20 kGy (in comparison with the 87660 kGy that a metallic component should absorb over a period of 1000 years considering a reference dose rate of 10 Gy h^{-1}.

2.4. Hydrogen measurements

Hydrogen (H_2) is measured with a gas chromatograph VARIAN 450-GC. High purity helium is used as the carrier gas with a pressure of 200 kPa. The analyzed gas sample volume is 1 mL. The column is a Molecular Sieve 5A (length = 3m and diameter = 3.17 mm). The detection is performed using a Pulsed Discharge Helium Ionization Detector (PDHID detector). The GALAXIE software (Galaxie chromatography Data System) is used to collect data. Calibration of the detector is performed by injection of a mixture of $H_2/O_2/N_2$/He gas (gas mixture X50A, AirProducts) and uncertainty associated to gas measurement is estimated to be less than 10%. Accordingly to a predetermined analytical sequences, hydrogen production relative to each cell is independently measured every 20 minutes before, during and after irradiation period. This measurement is performed on 1 mL of gas which is sampled from the system and analysed by the gas chromatograph. Such measurement allowed to know the exact amount of H_2 (ppm) contained in this 1 mL gas sample and after a conversion, one can obtain the number of H_2 nanomoles present in this 1 mL gas sample. Since carrier gas (He) circulates at a flow rate fixed at 5 mL min^{-1}, the number of H_2 nanomoles is multiplied by a factor 5 to obtain the number

191 of H_2 nanomoles generated by the experimental system during a 1-minute period (nmol min^{-1}). Once
192 irradiation phase stopped, cell containing only ultrapure deaerated water is disconnected from the
193 circulation system whereas cell containing metallic samples and ultrapure deaerated water remains
194 connected for some days more. Corrosion rate is estimated due to the precise measurement of molecular
195 hydrogen production in the cells. By subtracting the H_2 production associated to the cells containing
196 only pure deaerated water (cells A2 and B2) from the one generated by the cells containing pure
197 deaerated water and metallic samples (cells A1 and B1), it should permit to estimate the volume of
198 hydrogen generated only by the process of anoxic corrosion under irradiation during a 1-minute period
199 (nmol min^{-1}). At this point, it should be mentioned that the potential impact on H_2 production induced
200 by the additional water/glass surface interface arising from the sample holder, present only in the cells
201 A1 and B1, is assumed to be quite limited and is not considered in our calculation. The corresponding
202 number of H_2 nanomoles that are generated by our experimental system in a 1-year period (nmol $year^{-1}$) is calculated and associated to the total surface area of our metallic samples to obtain the number of
204 H_2 nanomoles produced by the anoxic corrosion of the metallic coupons during a 1-year period (nmol
205 m^{-2} $year^{-1}$). These H_2 production values (nmol m^{-2} $year^{-1}$) are then converted in corrosion rate (µm $year^{-1}$) values by using a conversion factor. This conversion factor is selected after the end of the experiment,
207 accordingly to the main corrosion product that is identified after structural characterization of the
208 sample's surface, as explained in previous study [21].

Commenté [LG1]: Lina's version

209 2.5. *Post mortem* analyses

210 At the end of the experimental tests, the cells are disconnected from the circulation system and moved
211 into the glove box to be dismantled in order to collect the carbon steel coupons and the solutions under
212 anoxic conditions.

213 2.5.1 Liquid samples

214 pH values of the solutions are measured immediately after the opening of the cells using a pH meter
215 (Multi 3420, WTW) with a glass electrode (ADA S7/IDS, WTW). For the solution collected in the cell
216 containing only ultrapure deaerated water, the concentration of hydrogen peroxide (H_2O_2) is determined

in less than 24 hours after the end of the irradiation phase with the Ghormley triiodide method [22]. Two reagents are used: the first one is a mixture of potassium iodide (KI, VWR), potassium hydroxide (KOH, Fluka) and ammonium heptamolybdate ($(NH_4)_6Mo_7O_{24}$, VWR), and the second one is a buffer mixture (pH = 6) of potassium phthalate ($C_8H_4K_2O_4$, Merck) and phthalic acid ($C_8H_6O_4$, Merck). For a total volume of 3 mL, 750 µL of both reagents are mixed with 1.5 mL of the sampled solution. After ten minutes of reaction, the concentration of H_2O_2 is indirectly determined by measurement of I_3^- absorbance with the UV-VIS spectrophotometer UV-2600 (Shimadzu). For the studied solution, at ambient temperature, the molar extinction of I_3^- at the 348 nm wavelength is estimated at 25800 L mol^{-1} cm^{-1}. For the solution collected in the cell containing both ultrapure deaerated water and metallic samples, the concentration of total dissolved iron (Fe_{tot}) is measured after acidification (HNO_3) by Inductively Coupled Plasma Atomic Emission Spectroscopy (ICP-AES), using a iCAP 7600 Duo (Thermo Electron) apparatus. The concentration of silicon (Si) is also determined by ICP-AES.

2.5.2 Solid samples

During the dismantling of the experimental cell in the anoxic glove box, metallic coupons are collected, rinsed with ethanol and dried to prevent post-oxidation. They are then introduced into airtight boxes stocked inside the anoxic glove box. Out of the six coupons involved in each experimental test, two coupons are dedicated to microstructural characterization, two other coupons are used for weight loss measurement and corrosion rate estimation and the two last coupons are retained for additional analyses. One should note that all the analysed metallic samples have been submitted to irradiation and that no reference metallic sample (corroded without irradiation) has been studied in this work. Morphology and chemical composition of the corrosion products formed at the surface of the carbon steel samples are firstly investigated using a Scanning Electron Microscopy (SEM) coupled to Energy Dispersive Spectroscopy (EDS). Analysis is performed using a Field Emission Gun (FEG) JSM7000-F SEM apparatus (JEOL) under an accelerating voltage of 15 kV. Sample surface images are obtained using both Secondary Electron (SE) mode and BackScattered Electron (BSE) mode. EDS spectra are collected on point of interest using a silicon-drift detector (Bruker AXS). Samples are brought to the microscope in an airtight anoxic box and all subsequent transfers are done rapidly (less than one minute) to minimize

exposure to oxygen. For optical imaging and micro-Raman (µRaman) spectroscopy, metallic coupons are kept in airtight anoxic box equipped with a 1 mm thick glass window. Samples surfaces are imaged with an Olympus MX41 microscope equipped with a CCD camera. µRaman spectra are obtained using a LabRam HR800 spectrometer equipped with an Olympus MX41 microscope. YAG solid-state laser with wavelengths of 532 and 785 nm are used as excitation sources and power outputs are kept at reasonably low values (≈ 500 $\mu W/\mu m^2$) to limit thermal degradation.

2.5.3 Weight loss measurement

In the anoxic glove box, gravimetric measurements are performed on the dedicated metallic coupons which have been initially weighted. At the end of the irradiation phase, these coupons are weighted before and after being soaked in ultrasonic baths, with intermediate rinsing in deionized water between each bath. This operation is repeated until the weight stabilization of the coupons. Such soaking stages aim to remove the corrosion products present at the surface of the metallic sample without dissolving carbon steel material. The solution contained in the bath is composed of 50%m distilled water + 50%m HCl (37%, VMR) containing 5 g L^{-1} of hexamethylenetetramine ($(CH_2)6N_4$, VMR) as an inhibitor of iron dissolution under acidic conditions, and the duration of each bath is 5 minutes. The weight of the coupons is measured using a high accuracy mass balance (XP205DR, METTLER TOLEDO) to allow an estimate of the average general corrosion rate (r, in µm/y). The thickness (e, in µm) of metal damaged by corrosion is calculated according to (5):

$$e = \Delta m / (S \times \rho(Fe)) \quad (5)$$

where S is the surface area, Δm is the mass difference, and $\rho(Fe)$ is the iron density. The general corrosion rate r is given by (6):

$$r = e / t \quad (6)$$

where t is time (in year).

3. Results

3.1. Hydrogen gas generation and corrosion rate measurements

The evolution of hydrogen gas (H_2) production arising from the experimental cells tested during both Exp-A and Exp-B are shown in Figure 3. The evolutions of the temperature measured in the IRMA irradiation chamber during these two experiments are also reported in Figure 3. A comparison of the hydrogen gas generation associated with the two cells containing carbon steel samples immersed in pure deaerated water (A1-cell and B1-cell) is proposed in Figure 4.

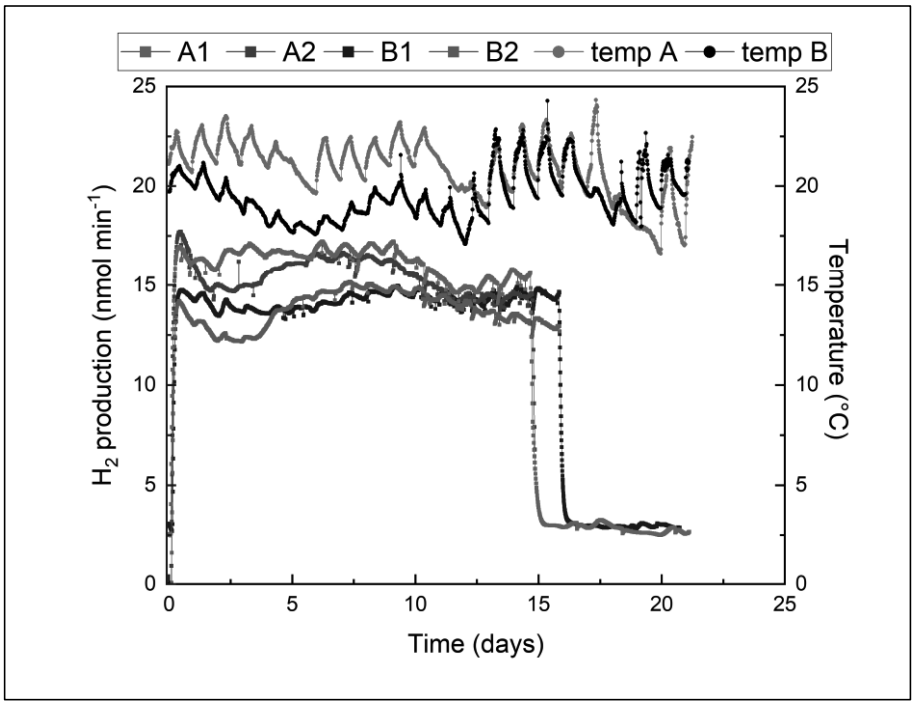

Fig. 3: Hydrogen productions evolution measured during the three studied phases (before, during and after irradiation) for experiments A and B with the associated temperature evolutions.

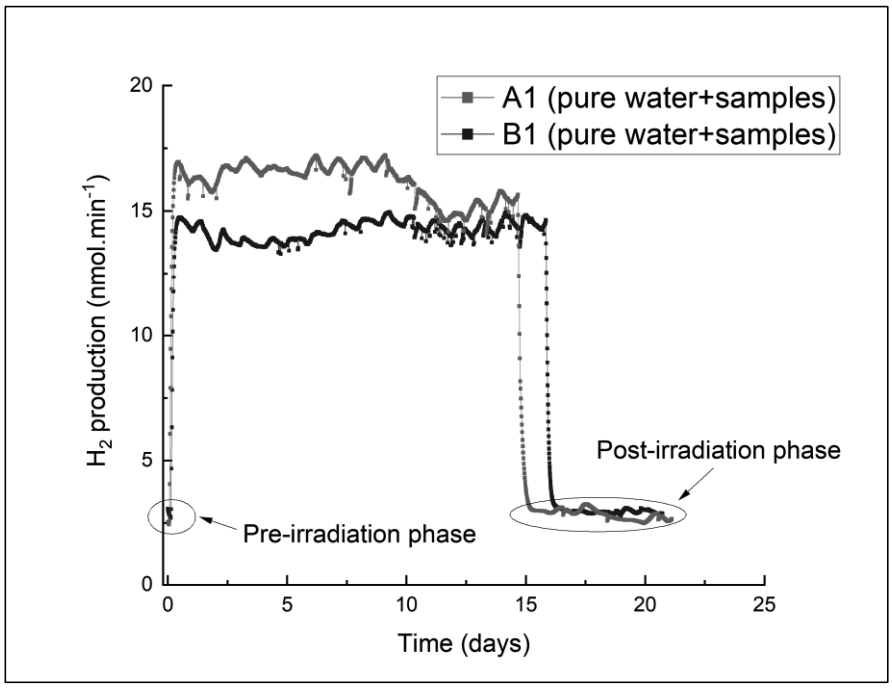

Fig. 4: Hydrogen productions evolution measured during the three studied phases (before, during and after irradiation) for cell A1 & B1 (ultrapure deaerated water and metallic samples).

For both cells, we can observe the very first H_2 production measurements performed before the irradiation phase that correspond to the hydrogen gas generated by carbon steel anoxic corrosion process. Then, the H_2 production measurements recorded during the irradiation phase correspond to the hydrogen gas generated by both water radiolysis and carbon steel anoxic corrosion processes. Finally, the last H_2 production results recorded after the irradiation phase correspond to the hydrogen gas generated by carbon steel anoxic corrosion process taking place post-irradiation. In parallel, Figure 5 presents the evolutions of the hydrogen gas produced by the two cells containing only pure deaerated water (A2-cell and B2-cell), which is exclusively generated by water radiolysis.

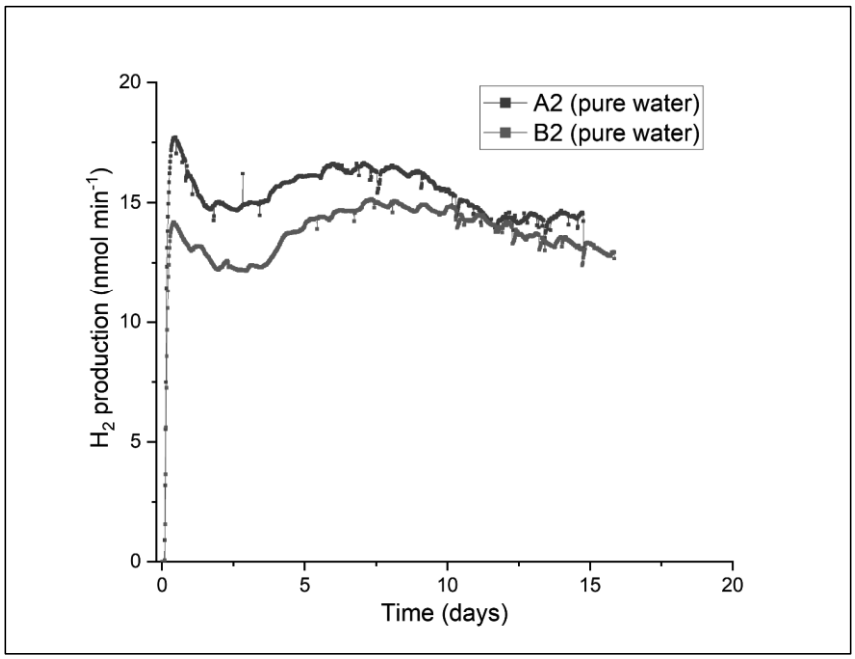

Fig. 5: Hydrogen productions evolution measured during the three studied phases (before, during and after irradiation) for cell A2 & B2 (ultrapure deaerated water only).

For all cells, the average and maximum values of hydrogen gas produced during the three tested phases (i.e., before, during and after irradiation) are given in Table 1. Average and maximum corrosion rates determined from these hydrogen gas generation are presented in Table 2. Table 3 presents the corrosion rate values that have been calculated from weight loss measurements performed either on 2 metallic samples for experiment A or on 1 metallic sample for experiment B.

cell	H_2 production before irradiation (nmol min^{-1})	H_2 production during irradiation (nmol min^{-1})	H_2 production post-irradiation (nmol min^{-1})
A1	2.5 ± 0.1	16.2 ± 0.7	2.8 ± 0.2
B1	2.8 ± 0.1	14.2 ± 0.4	3.0 ± 0.1
A2	0.0	15.4 ± 0.9	-
B2	0.0	13.8 ± 0.9	-

Table 1: Average values of H_2 production obtained for the three studied phases (before, during and after irradiation) of experiments A and B.

corrosion rate via H_2 gas measurements (µm $year^{-1}$)		before irradiation	during irradiation	post-irradiation
A1	Average	1.1 ± 0.1	0.3 ± 0.4	1.2 ± 0.1
	Maximum	1.1	1.1	1.4
B1	Average	1.2 ± 0.1	0.2 ± 0.4	1.2 ± 0.1
	Maximum	1.2	0.8	1.3

Table 2: Mean corrosion rate values (obtained *via* H_2 production monitoring) for the three studied phases (before, during and after irradiation) of experiments A and B.

corrosion rate *via* weight loss measurements (µm $year^{-1}$)	
A1 (2 metallic samples)	4.8 (± 0.3)
B1 (1 metallic sample)	1.9 (± 0.3)

Table 3: Mean corrosion rate values (obtained *via* weight loss measurements) for experiments A and B.

3.2. *Post mortem* analyses

3.2.1 Liquid samples

Once the irradiation stops, cells A2 and B2 were dismantled in the anoxic glove box. Hydrogen peroxide (H_2O_2) concentration measurement was performed within 24 hours after the end of irradiation for cell-A2 only, and the associated result is 0.52 x 10^{-6} mol L^{-1}. After the end of the experiment, A1 and B1 were also dismantled in the anoxic glove box. The collected solutions, showed a slightly grey coloration, were analyzed to determine the quantity of the released dissolved iron. In cells A1 and B1 the dissolved iron was measured in comparable concentrations at 0.34 mmol L^{-1} and 0.25 mmol L^{-1}, respectively. Furthermore, the initial and final values of pH were recorded in the glove box for each cell just before their closure and just after their dismantling. All the above mentioned measurements results are summarized in Table 4.

cells	**initial pH** (±0.2)	**final pH** (±0.2)	**[Fe_{total}] (mmol L^{-1})**	**[H_2O_2] (µmol L^{-1})**
A1	6.5	5.4	0.34 ± 0.01	-
B1	6.6	6.0	0.25 ± 0.07	-
A2	6.5	4.4	-	0.52 ± 0.09
B2	6.6	4.3	-	-

Table 4: Overview of the solution chemical characteristics. Initial and final pH values, final total iron concentrations ([Fe_{total}]) and final hydrogen peroxide concentration ([H_2O_2]).

3.2.2 Solid samples

After the end of the experiment, carbon steel samples have been structurally characterized as it is depicted on Figure 6. Metallic coupons collected in cells A1 and B1 exhibited a darker appearance regarding their initial state. We observed that this coloration is even more intense at the samples' edges. In comparison with the "roughly polished" samples (AR and BR coupons), the "mirror surface" samples (AP coupons) present a blurrier surface. Unfortunately, the first observation shows that the short duration of our experiments does not permit the formation of a thick and significant corrosion layer, as illustrated by the slightly corroded surface observed by optical imaging on "AR-coupon" (Fig. 6a), "AP-coupon" (Fig. 6b) and "BR-coupon" (Fig 6c).

339

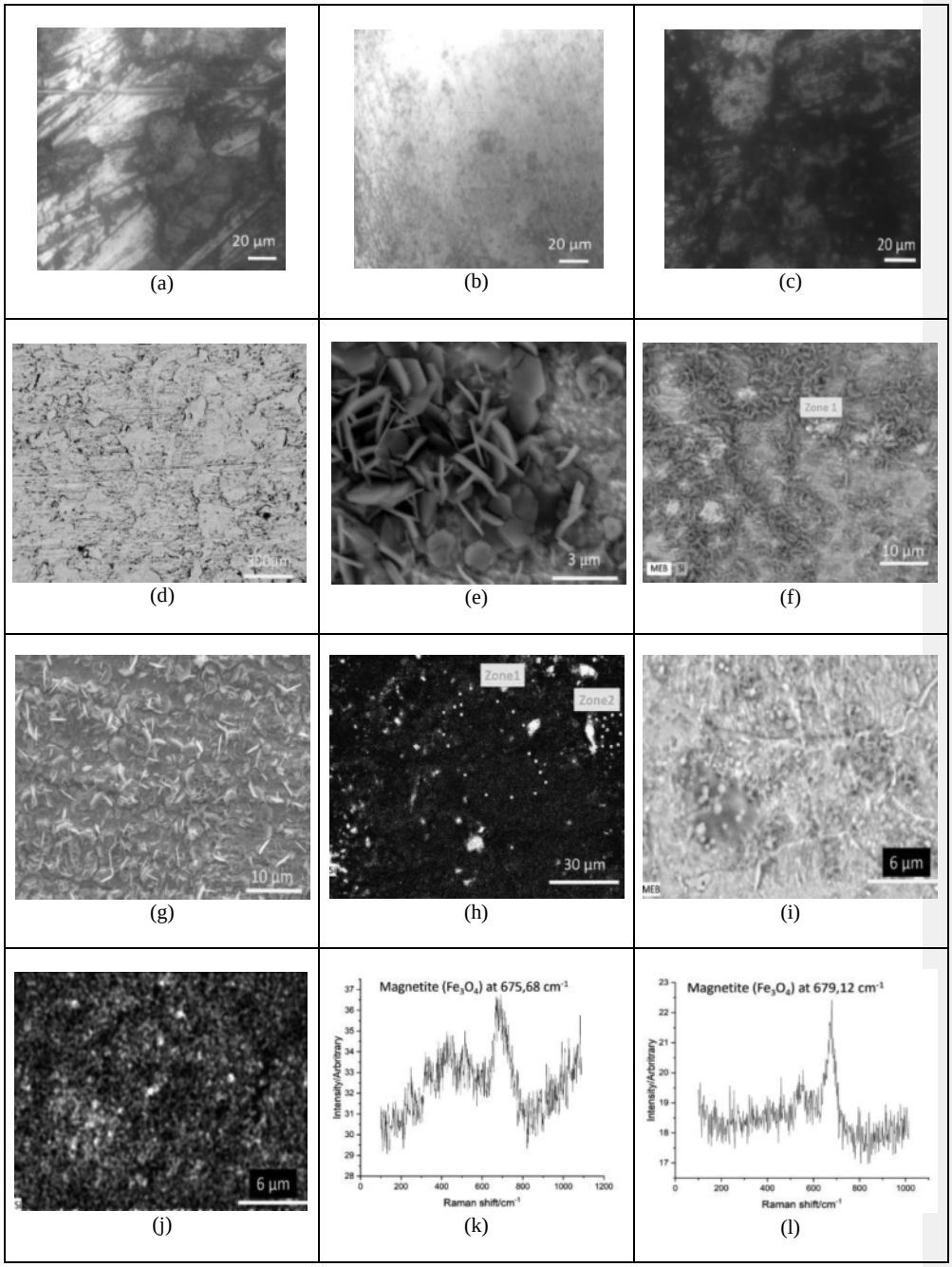

(a) (b) (c)

(d) (e) (f)

(g) (h) (i)

(j) (k) (l)

Fig. 6: Microstructural characterization of the carbon steel samples. Optical image of the corroded surface of AR-coupon (a), AP-coupon (b) and BR-coupon (c). SEM image in Backscattered Electron (BSE) mode of a roughly polished coupon before experiment (d), corroded surface of AR-coupon (e), corroded surface of BR-coupon (g) and corroded surface of AP-coupon (i). Composite BSE image – EDS elements map highlighting the areas enriched in Si on corroded surface of AR-coupon (f), corroded surface of BR-coupon (h) and corroded surface of AP-coupon (j). µRaman spectrum collected on the corroded surface of AR-coupon (k) and on the corroded surface of AP-coupon (l).

Surface examination using SEM-FEG microscopy have been performed on the surface of the metallic samples using Back Scattered Electron (BSE) as well as Secondary Electron (SE) mode. When comparing the initial surface of a roughly polished sample (Fig. 6d) with the final one of "AR-coupon" (Fig. 6e) and "BR-coupon" (fig 6g), we observe the formation of corrosion products mainly composed of hexagonal-shaped magnetite nanoplates. Surprisingly, such crystals formation has not been identified for "AP-coupon" (Fig 6i). Associated µRaman analyses indicated the presence of magnetite (Fe_3O_4), with a characteristic peak at 675.68 cm^{-1} and at 679.12 cm^{-1}, as the only identified corrosion product for "AR-coupon" (Fig. 6k) and "AP-coupon" (Fig. 6l) respectively. On the other hand, it was not possible to identify any corrosion product for "BR-coupon", even though, fine hexagonal-shaped formations observed in Fig. 6g. Moreover, it is worth mentioning that for both "AR-coupon" (Fig. 6f) and "BR-coupon" (Fig. 6h), elemental mapping revealed the presence of a significant amount of silicon (Table 5).

	Composition (at.%)					
	C	**O**	**Na**	**Si**	**S**	**Fe**
AR-coupon (zone 1)	6.6	51.2	0.2	11.9	0.1	29.9
BR-coupon (zone 1)	9.2	37.7	-	4.1	-	48.7
BR-coupon (zone 2)	12.4	13.3	-	0.1	2.2	72.0
AP-coupon	8.8	24.8	0.1	0.8	0.1	65.3

Table 5: EDX analyses of selected zones for AR-coupon, BR-coupon and AP-coupon. Selected zones are illustrated in Fig. 6.

4. Discussion

This study made possible to assess the quantities of H_2 produced by two parallel systems (cell-1 containing six carbon steel samples immersed in pure deaerated water and cell-2 containing only pure deaerated water) before, during and after irradiation under anoxic conditions and at ambient temperature. Hydrogen productions associated to each system which have been measured during two successive series of experimental tests (Exp-A and Exp-B) indicate quite reproducible results for the three studied phases (before, during and after irradiation) (Fig.3), allowing us to validate our experimental setup.

Before irradiation, hydrogen production associated with the cells containing only pure deaerated water (A2 and B2) remains zero, as expected (Fig.5). During this short pre-irradiation phase, the average H_2 production measured for the cells containing carbon steel samples (A1 and B1) is in the range of 2.5 - 2.8 x 10^{-9} mol min^{-1} (Fig.4). These fluxes of hydrogen, which are generated only through anoxic corrosion process, can be convert into corrosion rate values using a conversion factor [21] relevant for anoxic corrosion mechanism leading to the formation of magnetite (Fe_3O_4) as main corrosion product (*vide infra*). The corresponding calculated corrosion rate values range between 1.1 and 1.2 µm $year^{-1}$. Such values are in good agreement with literature data obtained in anoxic conditions and at near neutral pH, using ultrapure deaerated water [23], synthetic clay/granitic porewater [7-8], or numerical simulation with porewater [24], for greater time scales.

Commenté [LG2]: Lina's version

Once the irradiation phase starts, water radiolysis process takes place in cells A2 and B2, and we can immediately observe an intense production of H_2 (Fig.5). This is mainly due to recombination reactions occurring between hydrogen radicals and hydrated electrons [25]. According to Pastina et al. [26] the reactions (7), (8) and (9), which highlight the importance of hydrated electron (e_{aq}^-) and H radical ($H^\bullet$) regarding molecular hydrogen formation, are responsible for the majority of H_2 formation:

$$e_{aq}^- + e_{aq}^- + 2\,H_2O \rightarrow H_2 + 2\,OH^- \qquad k = 0.55 \times 10^{10}\ M^{-1}s^{-1} \qquad (7)$$

$$e_{aq}^- + H^\bullet + H_2O \rightarrow H_2 + OH^- \qquad k = 2.50 \times 10^{10}\ M^{-1}s^{-1} \qquad (8)$$

$$H^\bullet + H^\bullet \rightarrow H_2 \qquad k = 0.78 \times 10^{10}\ M^{-1}s^{-1} \qquad (9)$$

Since we consider the case of gamma rays in this experiment, we assume these reactions occur in spurs following the ionization processes [27]. As a result, G-values represent the primary yields of water radiolysis species in the beginning of the homogeneous stage. The initial slope of the intense increase of H_2 should correspond to the H_2 G-value, under γ-rays, 4.6×10^{-8} mol J^{-1} [28]. Using Figure 5 plots for pure deaerated water and the experimental parameters (dose rate of 50 Gy h^{-1}, measured volume of 1 mL), we have determined the initial slope of H_2-formation. We obtained 5.03×10^{-8} mol J^{-1} and 4.48×10^{-8} mol J^{-1} for A2 and B2 respectively, which roughly agrees with the literature. In parallel, H_2 can be consumed by reacting towards $^{\bullet}OH$ according to reaction (10):

$$^{\bullet}OH + H_2 \rightarrow H^{\bullet} + H_2O \qquad k = 4 \times 10^7\ M^{-1}s^{-1} \qquad (10)$$

but not in a big extent as this reaction is relatively slow and due to the fact that the use of a semi-open system does not permit to H_2 gas to return to the liquid phase. A better explanation of the stabilization of H_2 production is the accumulation in the solution of a radiolytic species which can efficiently react with the precursors of H_2 i.e. e_{aq}^- and H atom as seen in reactions (7) to (9). This species in pure deaerated water, under gamma rays, is H_2O_2, since O_2 cannot accumulate due to a constant He-bubbling.

Moreover, H_2O_2 can be formed as primary radiolytic species; but it can be also formed from $HO_2^{\bullet}$ [29]. We can mention this eventuality in case of accidental inclusion of air in the system, since under gamma rays $HO_2^{\bullet}$ stems from the reaction of O_2 with e_{aq}^-. In deaerated water this mechanism is not relevant. The only pathway to form $HO_2^{\bullet}$could be the reaction $OH+H_2O_2$ that in fine produces H_2O and O_2, which is released into the atmosphere by bubbling. This might be relevant under high LET irradiation, e.g. alpha rays, [29] in the case of a real deep geological repository.

Commenté [LG3]: GB version

As shown in Fig.5, H_2 productions successively measured for cells A2 and B2 indicate quite similar evolution and correspond to average values of 15.4×10^{-9} mol min^{-1} and 13.8×10^{-9} mol min^{-1}, respectively. For both cells, the initial H_2 production peak related to the beginning of the irradiation phase is followed by a sharp decrease taking place during the first 48h. After this, we observe a stabilization phase (between day 2 and day 4) which is followed by a progressive increase (between day 4 and day 6) and then by a second stabilization period (between day 6 and day 10). The fact that the

similar bell-shaped trends that we notice in H_2 trends in the absence of metal are not in accordance with temperature evolution and there are not related to an accumulated pressure within the cell, makes us conclude that they should be more attributed to a kind of regulation, considering the presence of possible impurities. Impurities arising from anything in contact with the pure water solution could lead to interaction of very reactive radicals e.g., $^{\bullet}OH$ and this could impact hydrogen production, as the maintenance of a totally ultra-pure water system in practice is almost impossible. Finally, both cells display a progressive decrease of their H_2 production until the end of the irradiation phase. According to the literature, a possible explanation for this progressive H_2 decrease arises from the formation of other radiolytic products with compatible reaction rates. The major factor that could inhibit H_2 formation is the presence of hydrogen peroxide (H_2O_2). The latter, as its concentration rises, is able to scavenge the main precursor of hydrogen, i.e. the hydrated electron (e_{aq}^-) [30], as shown by reaction (11):

$$H_2O_2 + e_{aq}^- \rightarrow OH^- + {}^{\bullet}OH \qquad k = 1.6 \times 10^{10}\ M^{-1}s^{-1} \qquad (11)$$

and thus, to inhibit the formation of molecular hydrogen. H_2O_2 was still identified in solution after a few hours necessary to collect sample in the cell A2 just after the end of irradiation. This low concentration ($H_2O_2 = 0.52 \times 10^{-6}$ mol L^{-1}, see Table 4) is the H_2O_2 concentration remaining in solution after irradiation. Then it suggests that reaction (11) occurred during irradiation.

Even if it seems that the H_2 production is influenced by the temperature fluctuations (Fig.3), it is somehow difficult to definitely state on the real impact of temperature on hydrogen production. On the one hand, the decrease of the temperature recorded between day 11 and day 13 for Exp-A seems to induce a diminution of the H_2 produced in cell A2. On the other hand, the increase of H_2 production observed between day 4 and day 6 takes place during a temperature decrease suggesting that temperature has no strong impact on radiolytic hydrogen production, as it has been previously mentioned [25]. The hypothetic coupled fluctuation of both H_2 production and temperature values observed on Fig.3 is indeed due to an experimental artefact induced by the great sensitivity of the gas chromatograph PDHID detector to temperature variation. If such perturbation could modify somehow the values of H_2 production, it impacts the two studied cells in parallel and should not have any effect on the derived corrosion rate values.

As shown in Fig.4, hydrogen productions associated to cells A1 and B1 are also strongly impacted by the irradiation. Indeed, the volume of H_2 generated by anoxic corrosion of the carbon steel samples is added to the one produced by water radiolysis process. Hydrogen productions successively measured for cells A1 and B1 indicate quite similar evolution and correspond to average values of 16.2×10^{-9} mol min^{-1} and 14.2×10^{-9} mol min^{-1}, respectively. This could be due to the fact that Fe-ions are known for reacting with radiolytical species with competitive reactions and thus they are able to impact H_2 evolution. Fe-ions can scavenge H_2 precursors (e_{aq}^-) and thus lead to a H_2 decrease, but at the same time Fe-ions can also interact very fast with OH radical, inhibiting the probability of reaction (11) and promote an H_2 increase. Therefore, we could say that an overall outcome would be a more stable H_2 evolution over time in the presence of metallic surfaces. By subtracting H_2 production associated to the cells containing only pure deaerated water (cells A2 and B2) from the one generated by the cells containing pure deaerated water and metallic samples (cells A1 and B1), it should permit to estimate the volume of hydrogen generated only by anoxic corrosion process. Thus, the average corrosion rates calculated for A1 and B1 during the irradiation phase are 0.3 μm $year^{-1}$ and 0.2 μm $year^{-1}$, respectively. These corrosion rate values obtained under irradiation and for anoxic conditions are consistent with the ones in previous studies performed in such experimental conditions [14,23]. Furthermore, we observe that cells A1 and B1 display constant behaviors all along the irradiation phase without any significant corrosion rate increase. This stabilization may be attributed to the gradual formation of a thin corrosion product layer, mainly composed of magnetite as observed during the structural characterization of our samples (Fig.6), which passivate and protect the carbon steel coupons surface. The identification of magnetite as predominant corrosion product has previously been observed in several carbon steel anoxic corrosion studies performed either under un-irradiated conditions [6,8,9,31–34] or under irradiation [14,23,35–37]. In previous studies dealing with long term anoxic corrosion under irradiation [14,38] such progressive magnetite formation has been associated to corrosion rate decrease. On the other hand, the comparison between corrosion rate values obtained during irradiation (0.3-0.2 μm $year^{-1}$) and the ones gained during the short pre-irradiation phase (1.1-1.2 μm $year^{-1}$) suggests that the presence of gamma radiation inhibits the anoxic corrosion rate of carbon steel. This is in contradiction with studies

Commenté [LG4]: Addition by linas version comment 33

comparing irradiated and un-irradiated samples [13,14,16,17,23] suggesting that ionizing radiation leads to a clear enhancement of the corrosion rate.

As soon as irradiation stops, hydrogen production associated to cells A1 and B1 falls until its stabilization at values around 2.8×10^{-9} mol min^{-1} and 3.0×10^{-9} mol min^{-1}, respectively (Fig.4). These volumes of hydrogen are generated only through anoxic corrosion process, and they allow to calculate corresponding anoxic corrosion rate, approximately at 1.2 µm $year^{-1}$ for both experiments. When comparing these results with the ones obtained during the pre-irradiation phase, we do not observe any diminution suggesting that, despite the primary and partial formation of a thin magnetite layer on the surface of the metallic samples, anoxic corrosion process continues to operate at the same rate that as before irradiation. This could be due to a progressive alteration of the primary formed magnetite layer which no longer protects the metal surface from further corrosion. The alteration could be caused by radiolytic-induced modifications of the solution. For example, the acidification of the solutions contained in cells A1 and B1 (see Table 4) could be due to the fact that under irradiation hydronium ions are produced in larger quantities than hydroxide ions. In the modelling work performed by Lapuerta [39], to explain the pH decrease that she observed experimentally (from 6.5 to 4.5), the author used primary radiolytical yields of α-rays ($g(H^+)$ = 0.37 x 10^{-7} mol J^{-1} and $g(OH^-)$ = 0.06 x 10^{-7} mol J^{-1}) corresponding to a mean LET value associated to a 2 MeV proton. Similarly, Christensen & Bjergbakke [40], propose primary radiolytical yields for low LET associated to gamma radiation with values at 2.85 x 10^{-7} mol J^{-1} and 0.10 x 10^{-7} mol J^{-1} for H^+ and OH^-, respectively. However, simulation results show that the H^+ concentration increase is not sufficient and the author proposed the contribution of additional ferrous/ferric ions hydrolysis processes to explain the observed pH diminution [39]. Additionally, the pH decrease due to the radiolytic oxidation of ferrous ions under gamma irradiation is also confirmed by Sutherland et al. [41]. Moreover, focusing on the final pH value on cells A1, B1 we should have in mind that our pH measurements have been performed several days after the end of irradiation phase. Once irradiation stops, the concentration of radiolytic species is dramatically decreased, although, the most stable among them, is hydrogen peroxide (H_2O_2), able to oxidize ferrous ions available in bulk solution via Fenton reaction (12):

$Fe^{2+} + H_2O_2 \rightarrow Fe^{3+} + {}^{\bullet}OH + OH^{-}$ (12)

During post-irradiation phase, this reaction will generate hydroxide ions prone to contribute to the higher final pH values, compared with the pH values measured in the cells where there were no metallic samples. Hence, the measured acidification of the solution is lower in in the presence of iron compared to the one's measured in the cells with pure water, however, it could be sufficient enough to impact corrosion processes.

Commenté [LG5]: Lina s version on comment 38

Such acidification of the solution can affect the magnetite solubility and thus inhibits the formation of a significant corrosion product layer which would lead to a corrosion rate decrease. This observation is to put in perspective with the work of Daub [42], showing that, contrary to the un-irradiated samples exhibiting a constant oxide film growth, the magnetite film thickness obtained on the gamma-irradiated sample displayed an initial fast development and then rapidly stabilized over time. On the other hand, impact of ionizing radiations on corrosion process can also be attributed to the oxidizing water radiolysis products such (H_2O_2, O_2 or $^{\bullet}OH$) which are produced simultaneously with reducing water radiolysis species (H_2, e_{aq}^-). Their interactions with carbon steel and stainless steel are known to induce a metal corrosion potential increase, as has been described by an electrochemical study [15]. Demonstrating that even after the end of the irradiation, the corrosion potential of the steel did not return to its initial lower pre-irradiated value, this work also pointed out the possible long-term changes in the corrosion product layer properties induced by structural modification of the oxide film (e.g., aggregation and coarsening of magnetite particles caused by the continuous dissolution–precipitation processes induced by irradiation as it is proposed by Sutherland et al. [41]). Such deterioration could impact the porosity of the neoformed corrosion product layer and may lead to a less active passivation of the metal.

In parallel, other parameters linked to our experimental setup can potentially impact the stability of the neoformed magnetite layer. If we refer to the work of Brusch & Pearl [31], highlighting the almost linear dependence of corrosion rate on the velocity of the tested flowing system, one can imagine that the 5 mL min^{-1} flow rate used into our gas circulation system may participate to the constant removal of the corrosion product located at the liquid/solid interface.

In addition, it was pointed out by Platts et al. [9], that any loss of ferrous ions from the system, e.g. from either adsorption and/or precipitation phenomena, can impair the formation of a thick protective corrosion product layer and lead to a renewed corrosion process.

Due to the progressive glass alteration process, the use of glass beaker and glass sample holder may induce ion-exchange mechanisms between silicon and iron ions [44–46]. We thus decided to perform additional post-mortem analysis on these glass elements. Acidic attack realized on glass beakers showed that total iron concentration value obtained for A1 beaker is two orders of magnitude higher than the one associated to the pristine beaker, meaning that ferrous iron ions have been entrapped in the glass alteration layer as observed in previous studies [47,48]. This ion exchange between iron and silicon is further confirmed by both the presence of silicon on the surface of the metallic coupons (Fig. 6 and Table 5), and the presence of silicon in solutions collected in A1 and B1 cells (results not shown).

From a radiolytical point of view, the densification of the borosilicate glass under gamma irradiation has been described in previous studies [49–52] to be a dose rate and boron content dependent process. In parallel, one can note that previous studies [53-55] showed that radiolytic yield of H_2 can be impacted in the case of oxide/water interfaces. Moreover, Schatz et al. [56], pointed out the fact that, during experiments dealing with silica suspensions under irradiation, the absorbed energy by silica nanoparticles crosses the solid/liquid interface and generates hydrated electrons in the aqueous phase as a result of an interfacial charge transfer process. This observation is in good agreement with the work of Nakashima & Tachikawa [57], where is mentioned the possible mechanism for hydrogen production by energy transfer from silica to the aqueous solution. The authors mention that a part of the initial hole/electron formation from irradiated silica can migrate in solids and reach the surface where they excite physisorbed water, leading to hydrogen formation. Therefore, we should note these parallel mechanisms potentially able to moderately affect hydrogen production arising from our experimental set-up involving irradiated glass. However, considering the low silica concentrations measured in our solutions, we consider that such processes involving silica nanoparticles should not significantly impact H_2 production.

548 Regarding the corrosion rates values estimated by weight loss measurements (4.8 µm year^{-1} for A test
549 and 1.9 µm year^{-1} for B test, see table 3), we observe that they are in the same order of magnitude as the
550 ones obtained during previous studies using the same technique [13,23]. Nevertheless, as mentioned in
551 previous studies [58–60] corrosion rates exported from weight loss measurements are higher than the
552 ones derived from the hydrogen gas generation measurements. Even though it is difficult to compare
553 instantaneous corrosion rate values obtained by H_2 gas generation monitoring with average corrosion
554 rate by weight loss measurements, such discrepancy would highlight that these two methods do not
555 monitor the same process. Moreover, one should mention that despite the anoxic conditions prevailing
556 in our experimental set-up, water radiolysis induced the production of reducing (H_2, e_{aq}^-) as well as
557 oxidizing (H_2O_2, $^{\bullet}OH$, O_2) species prone to modify locally physico-chemical conditions and to promote
558 in some extent oxic corrosion processes that are not associated to any H_2 gas production and for this
559 reason, they are not considered by our experimental approach which is based on H_2 monitoring.
560 Consideration of such information should support the concept of anoxic corrosion experiments based
561 on a twofold approach combining H_2 monitoring and weight loss measurements methods.

562 5. Conclusion

563 This work provides new insights on the impact of gamma radiation on carbon steel anoxic corrosion
564 process and on the associated H_2 gas generation. We adopted an experimental set-up based on the
565 hydrogen gas production monitoring which allows to distinguish between the H_2 production related to
566 water radiolysis and the one related to anoxic corrosion, making possible the estimation of associated
567 corrosion rate. Contrary to numerous previous results found in the literature, the first observation is that
568 gamma radiation does not induce a clear increase of the carbon steel corrosion rate but rather to slightly
569 inhibit it. This is probably due to the gradual formation of a thin magnetite layer which partially
570 passivates and protects the metallic surface. The second observation concerns the properties of
571 associated with such the magnetite layer and their evolution, during and after irradiation. Even though
572 corrosion rate under irradiation appears to be lower, the redox modifications of the solution induced by
573 radiolytic species production can induce the progressive alteration of the magnetite layer. This passive
574 film deterioration may maintain the metal surface in an active corrosion mode for longer period of time.
575 In parallel, the fact that the corrosion rate observed post-irradiation does not differ from the one

measured before irradiation also suggests the possible progressive degradation of the passivating corrosion product layer. This degradation could be due to oxidizing water radiolysis products which can induce structural modifications of the oxide film, either directly or through local modification of the physico-chemical conditions of the solution. If such sustained corrosion processes are verified, it could impact the degradation kinetic and the durability of metallic components used for HLW disposal gallery. Nevertheless, these assumptions need to be confirmed by further investigations performed with longer irradiation period and with more representative solutions (clayey pore water, alkaline pore water) in order to acquire an accurate understanding of gamma radiation impact on corrosion product growth and also on the evolution of oxide film properties. In parallel, numerical simulations should help to predict the concentration evolution associated to key radiolytic species prone to impact anoxic corrosion under irradiation processes and to better understand the effect of ionizing radiation in presence of metal/water interface or metal/oxide/water interface.

Acknowledgements

This work was supported by the French Institute of Radiation protection and Nuclear Safety (IRSN).

References

[1] D. G. Bennett and R. Gens, "Overview of European concepts for high-level waste and spent fuel disposal with special reference waste container corrosion," J. Nucl. Mater., vol. 379, no. 1–3, pp. 1–8, 2008.

[2] C. Padovani et al., "The corrosion behaviour of candidate container materials for the disposal of high-level waste and spent fuel–a summary of the state of the art and opportunities for synergies in future R&D," Corros. Eng. Sci. Technol., vol. 52, pp. 227–231, 2017.

[3] D. Crusset et al., "Corrosion of carbon steel components in the French high-level waste programme : evolution of disposal concept and selection of materials," Corros. Eng. Sci. Technol., vol. 2782, pp. 17–24, 2017.

[4] Andra, "Referentiel du site Meuse/Haute-Marne, Présentation Générale," Rap. C.RP.ADS.04.0022, Andra, Chatenay-Malabry, France, 2005.

[5] Andra, "Corrosion des matériaux métalliques," Tome 3, Rap. C.RP.ASCM.04.0015, Andra, Chatenay-Malabry, France., 2005.

[6] S. Necib, Y. Linard, D. Crusset, M. Schlegel, S. Daumas, and N. Michau, "Corrosion processes of C-steel in long-term repository conditions," Corros. Eng. Sci. Technol., vol. 52, pp. 127–130, 2017.

606 [7] M. L. Schlegel, F. Martin, M. Fenart, C. Blanc, J. Varlet, and E. Foy, "Corrosion of carbon steel in clay
607 compact environments at 90 °C: Effect of confined conditions," Corros. Sci., vol. 184, no. March, 2021.

608 [8] N. Smart, D. Blackwood, and L. Werme, "The anaerobic corrosion of carbon steel and cast iron in artificial
609 groundwaters," SKB Tech. Rep., 2001.

610 [9] N. Platts, D. J. Blackwood, C. C. Naish, S. N. Fuel, and W. M. Co, "Anaerobic oxidation of carbon steel
611 in granitic groundwaters: A review of the relevant literature," SKB Tech. Rep. 94-01, no. February, 1994.

612 [10] A. O. Allen, "The radiation chemistry of water and aqueous solutions," D. Van Nostrand Company, Inc.,
613 1961.

614 [11] G. V. Buxton, C. . Greenstock, W. P. Helman, and A. B. Ross, "Critical Review of Rate Constants for
615 Reactions of Hydrated Electrons, Hydrogen Atoms and Hydroxyl Radicals (.OH/.O−) in Aqueous
616 Solution," J. Phys. Chem. Ref. Data, 1988.

617 [12] V. Cuba, V. Mucka, and M. Pospisil, "Radiation Induced Corrosion of Nuclear Fuel and Materials," Adv.
618 Nucl. Fuel, 2012.

619 [13] G. P. Marsh and K. J. Taylor, "An assessment of carbon steel containers for radioactive waste disposal,"
620 Corros. Sci., vol. 28, no. 3, pp. 289–320, 1988.

621 [14] N. R. Smart, A. P. Rance, and L. O. Werme, "The effect of radiation on the anaerobic corrosion of steel,"
622 J. Nucl. Mater., vol. 379, no. 1–3, pp. 97–104, 2008.

623 [15] K. Daub, X. Zhang, J. J. Noël, and J. C. Wren, "Effects of γ-radiation versus H2O2 on carbon steel
624 corrosion," Electrochim. Acta, vol. 55, no. 8, pp. 2767–2776, 2010.

625 [16] N. Fujita, C. Matsuura, and K. Saigo, "Irradiation-enhanced corrosion of carbon steel in high temperature
626 water - In view of a cell formation induced by γ-rays," Radiat. Phys. Chem., vol. 58, no. 2, pp. 139–147,
627 2000.

628 [17] N. Fujita, C. Matsuura, and K. Saigo, "Radiation-induced preferential dissolution of specific planes of
629 carbon steel in high-temperature water," Radiat. Phys. Chem., vol. 60, no. 1–2, pp. 53–60, 2001, doi:
630 10.1016/S0969-806X(00)00326-1.

631 [18] E. Smailos, W. Schwarzkopf, R. Koster, B. Fiehn, and B. Halm, "Corrosion Testing of Selected Packaging
632 Materials for Disposal of High-Level Waste Glass in Rock Salt Formations," Kernforschungszentrum
633 Karlsruhe, KFK 4723, Karlsruhe, Ger., 1990.

634 [19] T. M. Ahn and P. Soo, "Corrosion of low carbon steel in concentrated synthetic groundwater at 80 to
635 150°C," Waste Manag., vol. 15, no. 7, pp. 471–476, 1995.

636 [20] B. Kursten et al., "Review of corrosion studies of metallic barrier in geological disposal conditions with
637 respect to Belgian Supercontainer concept," Corros. Eng. Sci. Technol., vol. 46, no. 2, pp. 91–97, 2011.

638 [21] N. Smart and A. Rance, "Effect of radiation on anaerobic corrosion of iron," SKB Tech. Rep. 05-05, 2005.

[22] A. O. Allen, C. J. Hochanadel, J. A. Ghormley, and T. W. Davis, "Decomposition of water and aqueous solutions under mixed fast neutron and gamma radiation," J. Phys. Chem., vol. 56, no. 5, pp. 575–586, 1952.

[23] H. Badet, "Effet de la radiolyse sur les systèmes de corrosion anoxiques à très long terme des alliages ferreux," Thesis, Univ. Pierre Marie Curie, 2014.

[24] M. Mohamed-Said, B. Vuillemin, R. Oltra, A. Marion, L. Trenty, and D. Crusset, "Predictive modelling of the corrosion rate of carbon steel focusing on the effect of the precipitation of corrosion products," Corros. Eng. Sci. Technol., vol. 52, pp. 178–185, 2017.

[25] Y. Tabata, Y. Ito, and S. Tagawa, CRC handbook of radiation chemistry. Boca Raton: CRC Press, 1991.

[26] B. Pastina, J. Laverne, and S. M. Pimblott, "Dependence of Molecular Hydrogen Formation in Water on Scavengers of the Precursor to the Hydrated Electron," J. Phys. Chem. A, vol. 103, no. 29, 1999.

[27] Y. Hatano, Y. Katsumura, and A. Mozumder, "Charged Particle and Photon Interactions with Matter," CRC Press, 2010, doi: 10.1201/b10389.

[28] J. W. T. Spinks, R. J. Woods, "An Introduction to Radiation Chemistry," Third Edition, John-Wiley and Sons, Inc., New York, Toronto 1990.

[29] G. Baldacchino, E. Brun, I. Denden, S. Bouhadoun, R. Roux, H. Khodja, C. Sicard-Roselli, "Importance of radiolytic reactions during high-LET irradiation modalities: LET effect, role of O2 and radiosensitization by nanoparticles," Cancer Nano 10, 2019.

[30] B. Pastina and J. A. LaVerne, "Effect of molecular hydrogen on hydrogen peroxide in water radiolysis," J. Phys. Chem. A, vol. 105, no. 40, pp. 9316–9322, 2001.

[31] E. Brusch and W. Pearl, "Corrosion and Corrosion Product Release Behavior of Carbon Steel," Proc. Am. Power Conf., vol. 31, pp. 699–705, 1969.

[32] J. Jelinek and P. Neufeld, "Kinetics of Hydrogen Formation From Mild Steel in Water Under Anaerobic Conditions.," Corrosion, vol. 38, no. 2, pp. 98–104, 1982.

[33] N. Senior, T. Martino, and N. Diomidis, "The anoxic corrosion behaviour of carbon steel in anoxic alkaline environments simulating a Swiss L/ILW repository environment," Mater. Corros., vol. 72, no. 1–2, pp. 131–140, 2020.

[34] N. Smart, A. Rance, and L. Werme, "Anaerobic Corrosion of Steel in Bentonite," Mat. Res. Soc. Symp. Proc. Vol. 807 ©, pp. 1–5, 2004.

[35] V. Cuba et al., "Radiolytic formation of ferrous and ferric ions in carbon steel - deaerated water system," Radiat. Phys. Chem., vol. 80, no. 3, pp. 440–445, 2011.

[36] N. R. Smart, A. P. Rance, D. J. Nixon, P. A. H. Fennell, B. Reddy, and B. Kursten, "Summary of studies on the anaerobic corrosion of carbon steel in alkaline media in support of the Belgian supercontainer concept," Corros. Eng. Sci. Technol., vol. 52, pp. 217–226, 2017.

673 [37] J. Vandenborre, F. Crumière, G. Blain, R. Essehli, B. Humbert, and M. Fattahi, "Alpha localized radiolysis
674 and corrosion mechanisms at the iron/water interface: Role of molecular species," J. Nucl. Mater., vol.
675 433, no. 1–3, pp. 124–131, 2013.

676 [38] N. R. Smart, B. Reddy, A. P. Rance, D. J. Nixon, and N. Diomidis, "The anaerobic corrosion of carbon
677 steel in saturated compacted bentonite in the Swiss repository concept," Corros. Eng. Sci. Technol., vol.
678 52, pp. 113–126, 2017.

679 [39] S. Lapuerta, "Etude de la corrosion du fer à l ' interface de différents milieux (eau , air) soumis à l '
680 irradiation de protons," Thesis, Univ. Claude Bernard - Lyon I, 2006.

681 [40] H. Christensen and E. Bjergbakke, "Application of chemsimul for groundwater radiolysis," Nucl. Chem.
682 Waste Manag., vol. 6, no. 3–4, pp. 265–270, 1986.

683 [41] T. I. Sutherland, C. J. Sparks, J. M. Joseph, Z. Wang, G. Whitaker, T. K. Sham, & J. C. Wren, "Effect of
684 ferrous ion concentration on the kinetics of radiation-induced iron-oxide nanoparticle formation and
685 growth," Phys. Chem., 19, 695-708, 2017.

686 [42] K. Daub, "A Study of Gamma Radiation Induced Carbon Steel Corrosion," Thesis, Univ. West. Ontario,
687 no. January, 2013.

688 [43] R. S. Glass, G. E. Overturf, R. A. Van Konynenburg, and R. D. McCright, "Gamma radiation effects on
689 corrosion-I. Electrochemical mechanisms for the aqueous corrosion processes of austenitic stainless steels
690 relevant to nuclear waste disposal in Tuff," Corros. Sci., vol. 26, no. 8, pp. 577–590, 1986.

691 [44] C. Carriere et al., "AVM nuclear glass / steel / claystone system altered by Callovo – Oxfordian poral
692 water with and without cement – bentonite grout at 70 ° C," Mater. Corros., 2020.

693 [45] T. Ducasse, "Apport des verres basaltiques à la validation du modèle GRAAL sur le très long terme,"
694 Thesis, Univerité de Montpellier, 2017.

695 [46] M. Fournier, S. Gin, and P. Frugier, "Resumption of nuclear glass alteration: State of the art," J. Nucl.
696 Mater., vol. 448, no. 1–3, pp. 348–363, 2014.

697 [47] H. Aréna et al., "Impact of iron and magnesium on glass alteration: Characterization of the secondary
698 phases and determination of their solubility constants," Appl. Geochemistry, vol. 82, pp. 119–133, 2017.

699 [48] P. Dillmann, S. Gin, D. Neff, L. Gentaz, and D. Rebiscoul, "Effect of natural and synthetic iron corrosion
700 products on silicate glass alteration processes," Geochim. Cosmochim. Acta, vol. 172, pp. 287–305, 2016.

701 [49] C. Allred, "Effect of radiation on silicon and borosilicate glass," Thesis, MIT, 2003.

702 [50] E. Birtch and J. Shelby, "Annealing of hydrogen-impregnated and irradiated vitreous silica," J. Non. Cryst.
703 Solids, vol. 349, no. 1–3, pp. 156–161, 2004.

704 [51] H. Manaktala, "An assessment of borosilicate glass as a High-Level waste form," Cent. Nucl. Waste Regul.
705 Anal. San Antonio, Texas, 1992.

[52] W. Primak, "Effects of ionization on silicate glasses," Nucl. Waste Manag. Mater. (UC-25), Argonne, Illinois, 1982.

[53] N. G. Petrik, A. B. Alexandrov, and A. I. Vall, "Interfacial Energy Transfer during Gamma Radiolysis of Water on the Surface of ZrO2 and Some Other Oxides," J. Phys. Chem. B, 105, 25, 5935–5944, 2001.

[54] P. Rotureau, J. P. Renault, B. Lebeau, J. Patarin, J. C. Mialocq, "Radiolysis of confined water: molecular hydrogen formation," Chemphyschem, 1316-1323, 2005.

[55] S. Le Caer, "Water radiolysis: Influence of oxide surfaces on H2 production under ionizing radiation," Water, 3(1), 235-25, 2011.

[56] T. Schatz, A. Cook, and D. Meisel, "Charge carrier transfer across the silica nanoparticle/water interface," J. Phys. Chem. B, vol. 102, no. 37, pp. 7225–7230, 1998.

[57] M. Nakashima and E. Tachikawa, "Self-radiolysis of Tritiated Water Adsorbed on Silica Gel," Appl. Radiat. Isot., vol. 37, no. 6, pp. 527–530, 1986.

[58] N. Diomidis, "Scientific basis for the production of gas due to corrosion in a deep geological repository," nagra, 2014.

[59] F. King, "Corrosion of carbon steel under anaerobic conditions in a repository for SF and HLW in Opalinus Clay," nagra, 2008.

[60] M. Kaneko, N. Miura, A. Fujiwara, and M. Yamamoto, "Evaluation of Gas Generation Rate by Metal Corrosion in the Reducing Environment," Eng. Report-Radioactive Waste Manag. Funding Res. Center(RWMC), no. RWMC-TRE-03003, p. 145, 2004.